nuclear fusion
IAEA

PAPER • OPEN ACCESS

Diagnosing fast ion redistribution due to sawtooth instabilities using fast ion deuterium-α spectroscopy in the mega amp spherical tokamak

To cite this article: A.R. Jackson *et al* 2020 *Nucl. Fusion* **60** 126035

OPEN ACCESS
IOP Publishing | International Atomic Energy Agency
Nuclear Fusion
Nucl. Fusion **60** (2020) 126035 (12pp)
https://doi.org/10.1088/1741-4326/abb619

Diagnosing fast ion redistribution due to sawtooth instabilities using fast ion deuterium-α spectroscopy in the mega amp spherical tokamak

A.R. Jackson[1,2], A.S. Jacobsen[2], K.G. McClements[2], C.A. Michael[3] and M. Cecconello[4]

[1] Department of Physics, University of Durham, South Road, Durham, DH1 3LE, United Kingdom of Great Britain and Northern Ireland
[2] CCFE, Culham Science Centre, Abingdon, Oxfordshire, OX14 3DB, United Kingdom of Great Britain and Northern Ireland
[3] Department of Physics and Astronomy, University of California - Los Angeles, Los Angeles, CA 90095-7099, United States of America
[4] Department of Physics and Astronomy, Uppsala University, SE-751 05 Uppsala, Sweden

E-mail: andrew.r.jackson2@durham.ac.uk

Received 23 June 2020, revised 17 August 2020
Accepted for publication 8 September 2020
Published 21 October 2020

Abstract

A comparison between fast ion measurements and sawtooth models in the Mega Amp Spherical Tokamak (MAST) is extended to include fast ion deuterium-alpha (FIDA) data. It is concluded that FIDA data cannot be used to distinguish between three alternative models used in the plasma transport/fast particle code TRANSP/NUBEAM to simulate fast ion redistribution during sawteeth. For FIDA lines-of-sight that probe the sawtoothing region, at each sawtooth crash there is an overall drop in the emission of up to 60%. Data from passive FIDA lines-of-sight (*i.e.* with emission resulting from neutralisation by thermal neutrals in the plasma periphery rather than beam neutrals) show a sudden increase in the emission following sawtooth crashes. The subsequent decay in the emission in these passive channels indicates that redistributed passing fast ions are rapidly lost from the edge region, probably as a result of charge-exchange reactions with edge neutrals.

Keywords: FIDA, fast ions, fast-ion deuterium-alpha spectroscopy, sawtooth instability

(Some figures may appear in colour only in the online journal)

1. Introduction

Sawtooth crashes arise from a periodic MHD instability found in tokamaks, wherein an internal kink instability with dominant toroidal mode number $n = 1$ and dominant poloidal mode number $m = 1$ forms due to a peaking of the plasma current profile (equivalently, the safety factor q drops below 1 in the plasma core region). This instability is characterised by a sudden flattening of temperature and density profiles in the core of the plasma [1]. The sawtooth instability and its interaction with the fast ion population is of interest to the development of ITER plasmas, as crashes can degrade the quality of the fast ion confinement or more generally cause redistribution in both configuration and velocity space, in particular an expulsion of fast ions from the sawtoothing region

[2]. ITER plasmas rely on good fast ion confinement as the primary source of heating comes from the fusion α-particles. The presence of fast ions can increase the amplitude of sawtooth crashes by stabilising the instability, delaying the onset of the crash and therefore causing its consequences to be more violent when it does occur [3, 4].

One of the tools that can be used to study sawtooth effects on fast ion confinement is fast ion deuterium-alpha spectroscopy (FIDA). The first such studies were carried out on the DIII-D conventional tokamak [5, 6]. Later the technique was applied to the investigation of fast ion behaviour during sawteeth in the ASDEX Upgrade conventional tokamak [7], and the inverse problem of determining sawtooth-induced changes in fast ion distributions from FIDA spectra has also been addressed in this device [8]. Most recently, FIDA has been used in conjunction with a solid-state neutral particle analyser to study the effects of sawteeth on fast ions in the NSTX spherical tokamak [9].

Plasmas in the Mega-Amp Spherical Tokamak (MAST) were heated by deuterium neutral beams with primary particle energies of typically around 60–70 keV and thus contained substantial fast ion populations whose behaviour could be studied using a range of diagnostics. The MAST data investigated in this paper have been previously examined by a number of researchers [10–12]. The study presented here extends the work carried out by M. Cecconello *et al* [12] and utilises TRANSP/NUBEAM data generated in the course of that study. Specifically, we have extended the data analysis to include FIDA data.

The structure of this paper is as follows: in section 2 the background regarding the diagnostic and modelling software used in the analysis is given; in section 3 the models used to describe the effect of sawtooth crashes on the plasma are discussed; in subsection 4.1 the different models are compared using the experimental and synthetic FIDA data; in subsection 4.2 further analysis regarding the redistribution of the fast ions in the experiment is described and in section 5 some preliminary results regarding the analysis of passive FIDA emission are presented.

2. Fast-ion deuterium-α spectroscopy

The FIDA spectroscopic diagnostic can be utilised to gather local measurements of the fast-ion distribution present in the plasma. The neutral-beam injection (NBI) system introduces high energy deuterium neutrals into the plasma which can undergo charge exchange reactions with the fast-ion population (resulting from the ionisation of beam neutrals), generating a fast neutral that can be in an excited state. De-excitation from quantum state $n=3$ to $n=2$ generates a Balmer-α photon. The wavelength of this photon is determined by the combined effect of a Doppler shift arising from the fast ion's line-of-sight velocity and Stark splitting arising from the presence of an electric field in the rest frame of the fast neutral [13]. The Stark splitting is a relatively small effect in spherical tokamaks such as MAST due to the low magnetic field. The observed spectrum also has other *active* (present only when the neutral beam is on) and *passive* (present whether the beam is on or off) spectral components that must be taken into account during interpretation. A component of the passive signal is FIDA light generated by charge exchange between cold edge neutrals and fast ions. Analysis of this is discussed further in section 5. This and other passive components such as bremsstrahlung can be subtracted from the raw signal. A toroidally displaced reference view (as was used on MAST [14]) observes plasma that does not contain a neutral beam. Assuming axisymmetry, this can be used to subtract from the main view to leave only the active signal. Alternatively, some tokamaks use beam notching, which requires instead the assumption of some degree of temporal stability. In order to interpret the data taken by the diagnostic, forward modelling is performed using the codes TRANSP/NUBEAM [15, 16] and FIDASIM [17]. TRANSP is a long-standing plasma transport and equilibrium solver that can be used to both analyse and predict plasmas. NUBEAM is a Monte-Carlo module for TRANSP that allows for the simulation of NBI systems and of the fast-ion populations that are generated. Profiles of a number of experimentally determined plasma parameters, such as (but not limited to) electron temperature and density, impurity density and toroidal plasma rotation at a particular time are given as input. A magnetic equilibrium is also required, which can be generated EFIT beforehand or can be evolved with TRANSP's internal solver. The plasma is evolved in time and produces simulated fast-ion distributions, which form the crucial input to FIDASIM. FIDASIM uses these distributions to generate a synthetic active FIDA spectrum, which can then be compared with the background-subtracted experimental data. Figure 1 shows a synthetic spectrum generated with FIDASIM, indicating the form of a typical active signal as observed on MAST in terms of specific components.

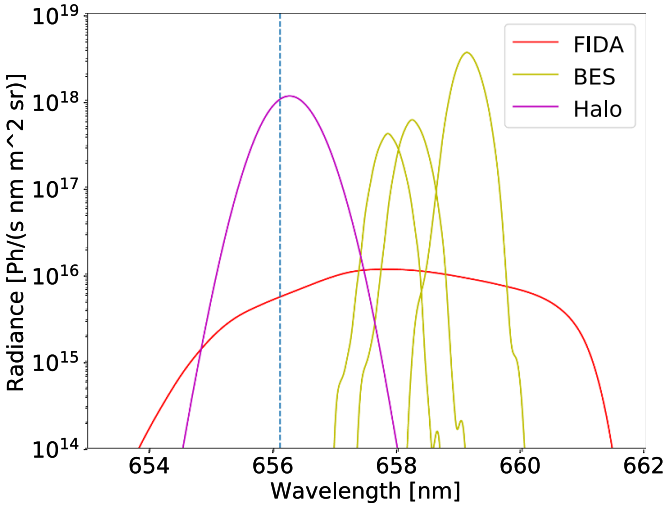

Figure 1. Example spectra generated with FIDASIM of the toroidal view on MAST showing the FIDA, BES and halo components of the spectra. The dotted vertical line shows the location of the rest wavelength of deuterium-α emission, 656.1 nm. The BES (beam emission spectroscopy) peaks are caused by collisional excitation of beam neutrals to $n=3$ states. There are three such peaks since the beam contains neutrals with energies equal to one half and one third of the primary energy.

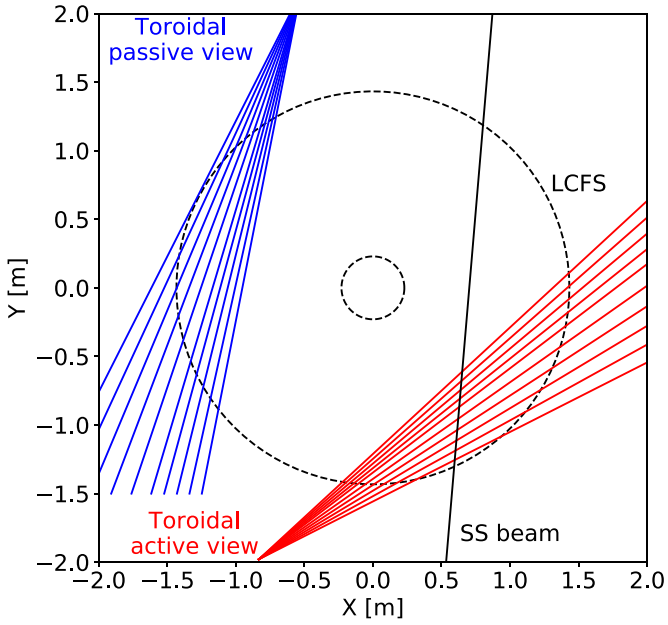

Figure 2. Plan view of MAST, showing an example last closed flux surface, along with the NBI beam and the relevant toroidal lines of sight.

Due to the specific geometry of the NBI system and the toroidally viewing FIDA diagnostic (the line-of-sight is co-current, as is the beam) the spectra is primarily red-shifted. The FIDA component is shown in red. The three peaks in yellow represent emission due to collisional excitation of injected neutrals (beam emission spectroscopy or BES). The location of the peak is dependent on the injection energy, with three peaks appearing due to there being a small proportion of di- and tri-atomic deuterium molecules in the NBI system, leading to full, half and third energy peaks. The halo component is generated by charge-exchange between the injected neutrals and the thermal ions. It may be noted that the halo component has a slight redshift, which is indicative of there being a bulk co-current rotation of the plasma. The MAST implementation of this diagnostic (described in detail in [14]) had both toroidal and vertical lines of sight, with associated passive views. Figure 2 shows the extent of the relevant toroidal views, along with the utilised NBI beamline and the last closed flux surface (LCFS). Due to the relative orientation of the lines-of-sight with respect to the magnetic field, toroidal views are primarily sensitive to passing particles, while vertical views are primarily sensitive to trapped particles.

3. Sawtooth models in TRANSP

The Kadomtsev model characterises the sawtooth crash as a process of rapid magnetic reconnection [18], in which equal and opposite helical flux on either side of the $q = 1$ surface (q being the safety factor) reconnect, forming a magnetic island that grows to become the new magnetic core of the plasma. The new core is colder and less dense than the original hot core, which is dispersed towards greater minor radii. In this model complete reconnection occurs - directly after the crash $q \geqslant 1$ everywhere in the plasma. Experimentally this model has been shown to be not applicable to all plasma pulses. Porcelli *et al* [19] describe a number of pulses, some of which follow the Kadomtsev model and several that do not. The authors then propose an alternative model (referred hereafter as the Porcelli model) which allows for incomplete reconnection, meaning that $q(r = 0) < 1$. Here the formation of the magnetic island begins as in the Kadomtsev model but is interupted by magnetic turbulence once the island has grown to some threshold size. The Kadomtsev model moves plasma at $q = 1$ pre-sawtooth to the magnetic axis after the sawtooth, and other regions are mixed with helical flux-matching as described above. This has a flattening effect on the temperature and density profiles, but can cause some previous structure to be retained. Alternatively, ergodic mixing can be utilised, ignoring the requirement of flux-matching and redistributing the plasma in such a way that the temperature and density profiles are completely flattened within the mixing region. Henceforth we refer to a model implementing this complete flattening of profiles as the ergodic model. The Porcelli model specifies two regions that are mixed separately, based on how large the magnetic island is allowed to grow before it is interrupted. Once the new locations for the markers have been determined, the post-crash equilibrium combined with conservation of magnetic moment and velocity parallel to the magnetic field determine the change in the energy and velocity of the markers [20]. TRANSP/NUBEAM implements the models in the KDSAW module, and a full explanation of the behaviour of the models is given in the online documentation [21]. Figure 3 shows synthetic spatial distributions of fast ions on MAST (generated by TRANSP/NUBEAM) before (figure 3) and after (figure 3) a sawtooth crash.

The three models (Kadomtsev, ergodic and Porcelli) were used in TRANSP/NUBEAM runs previously used in [12] to provide simulated fast-ion distributions before and after each sawtooth in pulse #29 880. These were then utilised, with FIDASIM, to generate synthetic spectra, which are compared to the experimental data.

4. Analysis

The data used in this study derive from a series of three pulses (#29 880-#29 882) which were designed to be as similar as possible. Figure 4 shows the time evolution of each pulse in a variety of parameters. The sawtooth crashes are clearly seen in the neutron rate and core electron temperature, but for these pulses the electron density is largely unaffected by the instability. To analyse the FIDA data, time slices were taken before and after the third sawtooth in the overall sequence of sawteeth. The EFIT equilibrium reconstruction yields a q-profile greater than 1 at the time of the first sawtooth, and is not low enough after the second sawtooth to trigger the Porcelli model. A q substantially less than 1 is required to trigger the 3 sawtooth models in TRANSP/NUBEAM, a condition that is met by the time of the 3rd sawtooth in the sequence. Additionally, there is a secular downward trend in the experimental FIDA radiance over the course of the pulses, so the

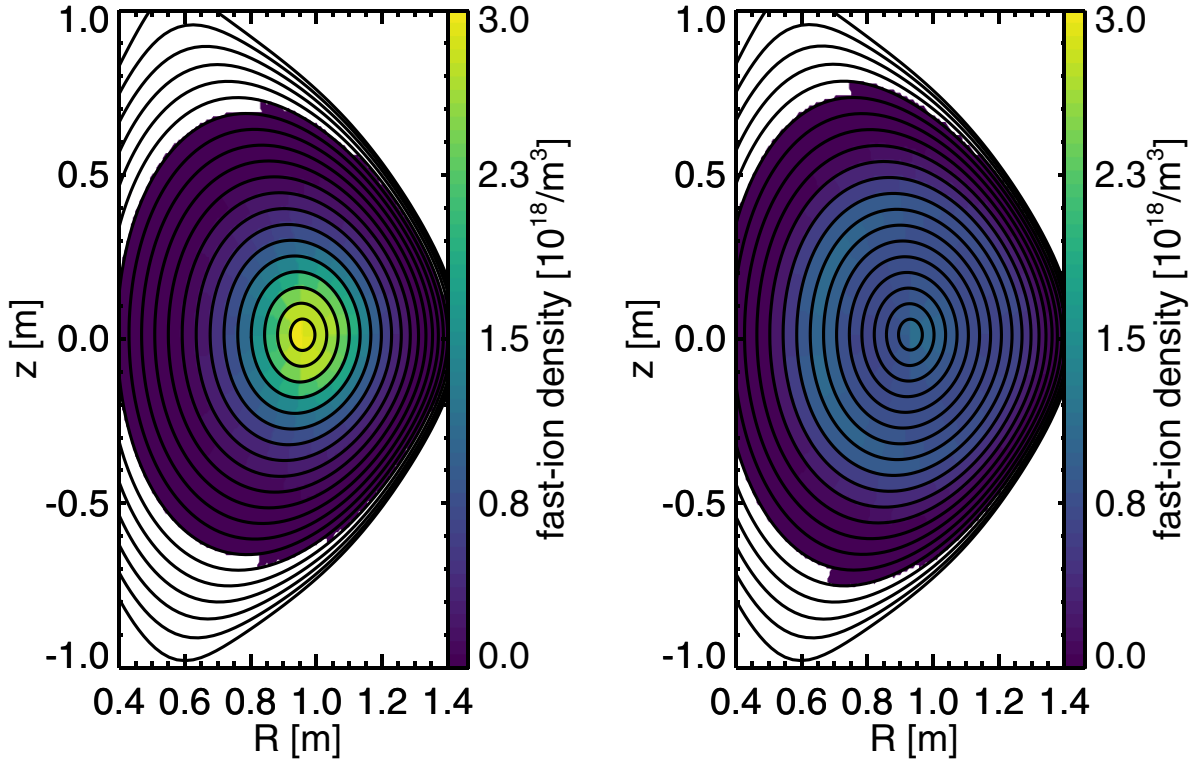

(a) Before crash. (b) After crash.

Figure 3. The simulated fast-ion density in an azimuthal cross section of MAST before and after a sawtooth crash, with the flux surfaces shown in black.

third sawtooth provides the best available signal-to-noise ratio. Figure 5 shows a soft x-ray (SXR) tangential camera trace, for a line-of-sight with a tangency radius of 0.528 5 m, before, during and after the selected single crash present in all three pulses. The SXR camera is uncalibrated, and the signal has units of volts. The soft x-ray emission can be regarded as a proxy for electron temperature.

The replication of the tokamak conditions between pulses is such that, in the sequence of crashes that occurs in all of the pulses, the selected crash is separated in time by a maximum of 7 ms between the pulses. This is significantly less than both the energy confinement time and the fast-ion slowing down time at around the time of the selected crash. From this it is concluded that the pulses are repeatable and that it is appropriate to average across pulses (after aligning the selected crashes in time) as well as averaging across time, thereby improving the signal-to-noise ratio. This technique was also used in the previous investigations [11, 12]. The BES peaks were extremely bright compared to the FIDA light, which can be problematic as there can be pixel-to-pixel 'bleeding' in the spectrometer charge-coupled device (CCD) chip in such situations. An optical mask was used to block these features. Figure 6 shows an example of the full experimental spectrum along with the corresponding FIDASIM prediction (using the Kadomtsev model only, as an example).

It can be seen that the presence of the other spectral components (and the mask) means that there are no usable data in the lower end of the wavelength range, and the signal decays rapidly towards the upper end. What remains is the usable window, highlighted in green. The position and size of the window in wavelength space varies across different imaged positions in the plasma (spectrometer *channels*), but in every case there is a region of the spectrum dominated by the fast ions.

4.1. Comparison of different sawtooth models with FIDA data

In the work of Cecconello and co-workers [12] neutron camera data were insufficient to determine which of the three sawtooth crash models used (Kadomtsev, ergodic and Porcelli) provided the best fit to the data. It was speculated that FIDA data may help in this regard. Figure 7 shows a before- and after-crash timeslice of the FIDA data, averaged over 3 ms (1–4 ms before crash, 1–4 ms after the crash) and across the three pulses (with the crash times aligned), along with synthetic spectra generated using each of the sawtooth models mentioned above, for a channel observing the plasma at a radius of 1.205 m in the plasma midplane. The corresponding plasma minor radius ρ (defined as $\rho = \sqrt{\psi_N}$, where ψ_N is the normalised poloidal flux) is 0.569, 0.565 and 0.58 before the crash and 0.573, 0.57 and 0.584 after the crash for the Kadomtsev, ergodic and Porcelli models respectively. The synthetic data were only generated for pulse #29 880. It is appropriate to do this for the reasons given at the beginning of this section (4), *i.e.* that the plasma conditions are closely replicated in the three pulses that are analysed.

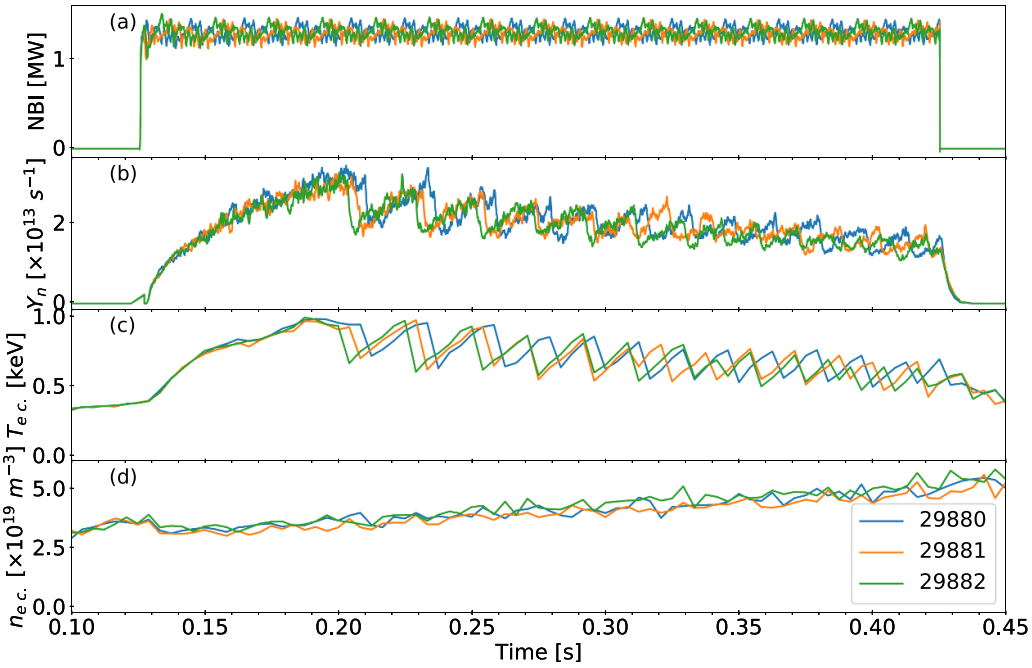

Figure 4. Time traces of plasma parameters for the three pulses used in averaging. (*a*) NBI power, (*b*) neutron rate, (*c*) core electron temperature, (*d*) core electron density.

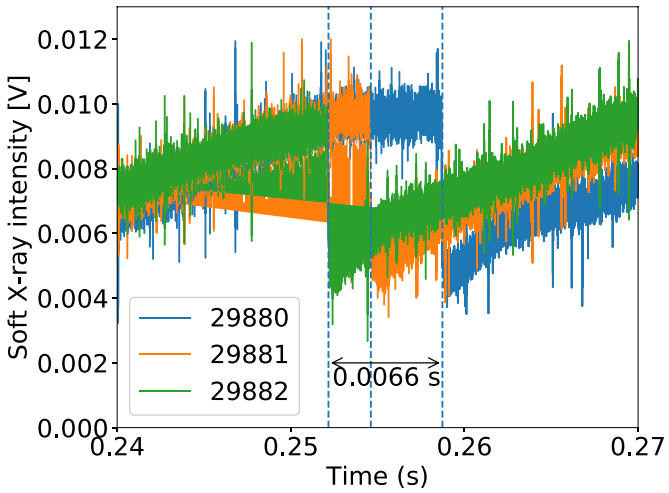

Figure 5. Soft x-ray (SXR) trace (for a line-of-sight with tangency radius 0.5285 m) showing a sawtooth crash for shots #29 880, #29 881 and #29 882.

Before the crash there is a difference between the predicted spectra. As mentioned previously, due to the equilibrium reconstruction used, none of the models trigger at the time of the first sawtooth, and only the Kadomtsev and ergodic model trigger at the second sawtooth. Therefore we observe a small difference in the models before the crash. Drops in spectral radiance are observed in both the experimental and synthetic data for the channel shown in figure 7 and for channels closer to the core, with channels further out showing small to no drop. The absolute values for the spectral radiance is reproduced well by the TRANSP/NUBEAM and FIDASIM modelling, for the shown channel in figure 7. However, this degree of agreement is only seen in the shown channel; other channels show serious deviation between experiment and prediction, an example of which is given in figure 8. This figure shows the same region of wavelength space as figure 7 but for a channel at R = 1.139 m (corresponding to pre-crash normalised minor radii $\rho = 0.419$, 0.414, 0.435, and post-crash radii $\rho = 0.425$, 0.42, 0.44 for the Kadomtsev, ergodic, and Porcelli models respectively) in the plasma midplane.

This discrepancy in the absolute magnitude, possibly due to calibration factors, is discussed further in section 4.2. An EFIT equilibrium with a lower core q would lead to a larger sawtoothing region, and so more fast ions would be expelled by the crash. This would imply a lowering of the FIDASIM spectrum within the sawtoothing region, and an increase outside it, potentially giving better agreement between the absolute magnitudes of the experimental and synthetic spectra. In all channels, over most of the usable wavelength space, the 3 sawtooth models produce only a small difference in the predicted spectra compared to the overall change due to the sawtooth. The errors shown are based on the combination of photon shot noise and the CCD read noise for both the active and passive channels used (dark current noise is neglected due to the cooling of the CCD chip). It must be emphasised that this represents the minimum possible error on the FIDA data and that the true error may be larger, especially considering the possible problems due to uncertain calibration, discussed in subsection 4.2. Due to this uncertainty and the size of the error, no clear determination of the suitability of one model over the others can be made. We conclude that FIDA measurements cannot resolve the issue of which model best represents the data [12].

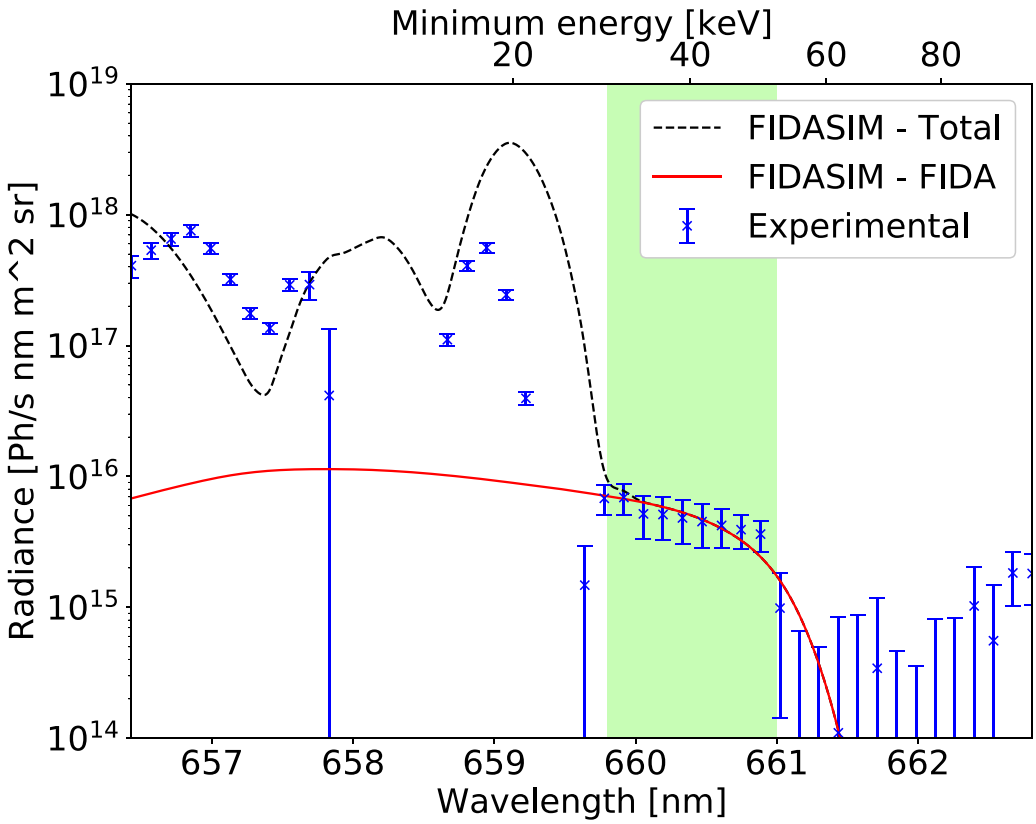

Figure 6. An example of the full redshifted experimental D-α spectrum for pulse #29 880 along with the corresponding synthetic pre-sawtooth spectrum, showing the summation of all the synthetic components and the synthetic FIDA component in isolation. The shaded area shows the extent of the experimental spectrum that is usable for analysis. All other wavelength regions are unusable for fast ion studies due to an optical mask blocking bright unwanted regions of the spectra, unwanted spectral components dominating the FIDA component, or the lack of any fast ion signal at all.

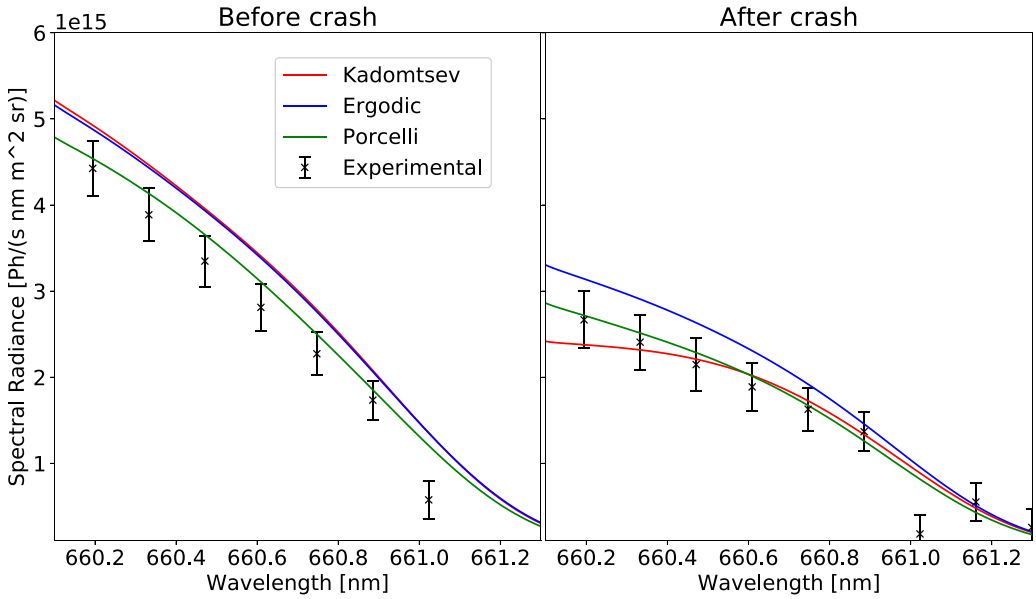

Figure 7. Experimental and synthetic spectra showing only the region where FIDA light can be observed at R = 1.205 m in the plasma midplane. The predictions based on the three models are shown.

4.2. Detailed analysis of fast-ion redistribution by sawtooth crash and comparison with FIDA

While in the previous section is was shown that FIDA is not sensitive enough to distinguish between the three sawtooth models, and that there was significant deviation of the experiment and prediction, by eliminating a source of calibration error it is shown in this section that we can achieve good agreement between the forward-modelled FI redistribution due to

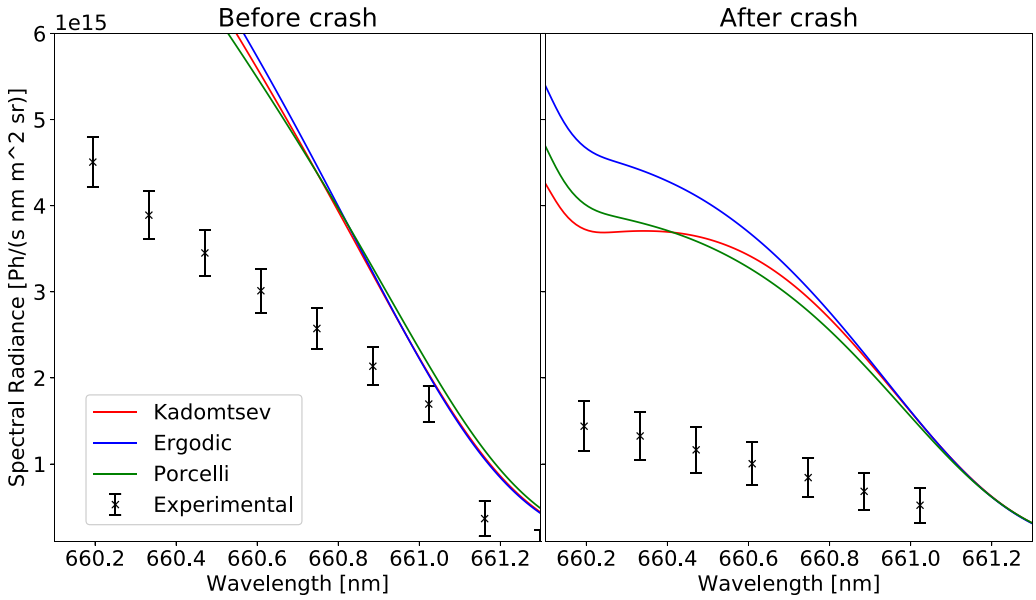

Figure 8. Experimental and synthetic spectra showing only the region where FIDA light can be observed at R = 1.139 m in the plasma midplane. The contribution to the spectrum from the full energy BES peak can be seen at the lower wavelengths, but the discrepancy between the experimental and synthetic spectra persists to higher wavelengths.

the sawtooth crash and the diagnostic within the experimental error. Only some of the FIDA channels contain usable spectral data. Channels close to the plasma edge view plasma regions containing relatively few fast ions and those close to the plasma core view plasma regions containing few neutrals with which the fast ions can charge exchange. Both of these effects lead to a low level of FIDA radiance. Of the channels with a usable level of FIDA radiance it was observed that only a single channel, observing the plasma at a major radius of 1.205 m, consistently showed agreement between the absolute experimental values and the FIDASIM predictions. However, it has been shown previously that a scaling factor is required in order to model the experimental BES peaks correctly [14]. Applying that factor here would lead to larger disagreement between the model and data, and would have varying effects on the agreement in the other channels. Due to the presence of the optical mask it is not possible to use the comparison of the experimental and synthetic BES peaks here as a test of the calibration and scaling validity. Investigating relative changes in the spectra between pre- and post-crash reduces or eliminates some of the effects of absolute miscalibration. Figure 9 shows the relative change (difference in signal after the crash vs before, divided by the signal before) in the observed spectral radiance across the fast-ion dominated portion of the spectrum, across channels that have an observable level of FIDA radiance averaged using the same methods described for figure 7 above.

The location of the BES peaks in wavelength space are dependent on the relative orientations of the line-of-sight to the NBI beamline, so they appear at different locations in wavelength for the different FIDA channels, which can reduce the usable areas of the spectrum. The sawtooth crash affects the BES peaks due to changes in the beam deposition profile. Unusable parts of the spectra due to this effect are shown by the greyed out portions in figure 9. These were determined by calculating the relative change in the synthetic spectra before and after the sawtooth crash firstly using all FIDASIM spectral components and again with only the FIDA component. A region of the wavelength range was designated as unusable if the difference between these two calculations was greater than 0.5% in terms of the vertical scale used in figure 9. The figure of 0.5% is somewhat arbitrary, but was chosen to ensure that sawtooth-induced changes in the BES peaks (which were not caused by fast ion redistribution) did not have a significant effect on the overall change in the measured intensity. Note as well that the error on the experimental data increases significantly at wavelengths above 661.0 nm, as the absolute signal experiences a rapid drop-off. It can be seen that in the valid region the experimental and synthetic results are comparable for the most part except at 1.139 m (figure 9(*d*)), where there is significant disparity between them. Through examination of Thomson scattering data, it can be determined that the outboard radius of the inversion region in the midplane is approximately 1.16 m (corresponding to pre-crash normalised minor radii $\rho = 0.467$, 0.462, 0.481, and post-crash radii $\rho = 0.472$, 0.468, 0.486 for the Kadomtsev, ergodic and Porcelli models respectively), slightly higher than the tangency radius corresponding to figure 9(*d*) and slightly lower than that corresponding to figure 9(*e*). Comparing these two plots, it can be seen that the relative change in emission following the sawtooth crash is considerably larger in figure 9(*d*) than it is in figure 9(*e*). This in itself is unsurprising, since the effects of the sawtooth on the emission are expected to become smaller as the line of sight moves away from the sawtoothing region. The fact that an effect is seen at all in figure 9(*e*), despite the tangency radius lying outside the sawtoothing region, can be explained by the fact that the fast ion orbit widths and Larmor radii are typically larger than the difference between the

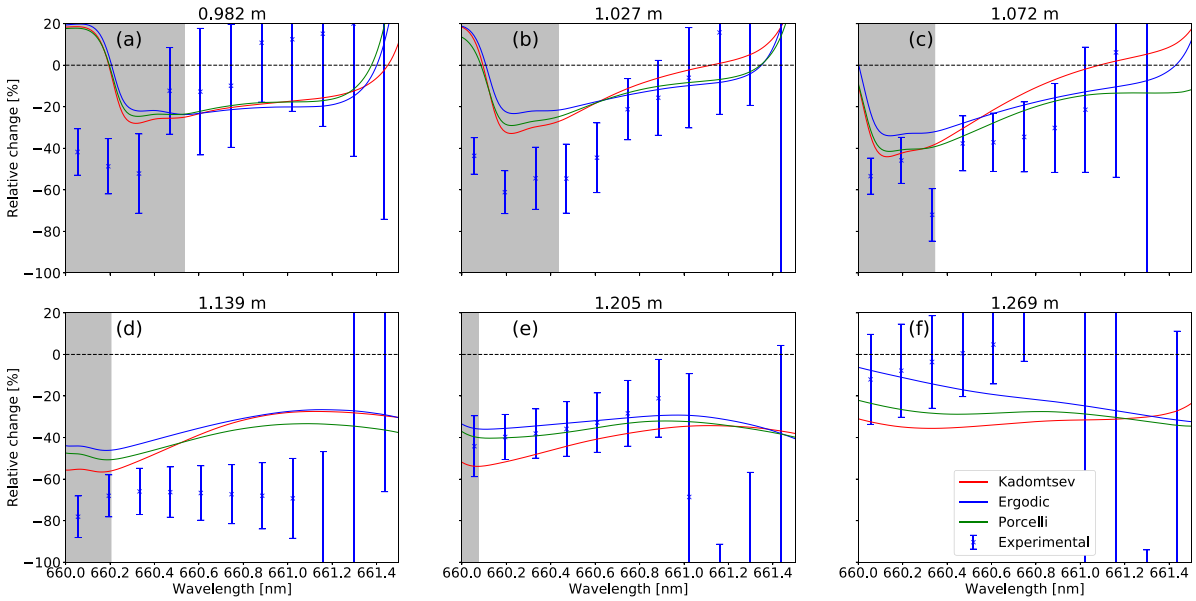

Figure 9. Spectral radiance across a number of FIDA channels. Note that the full energy BES peak appears at different locations depending on channel. The grey shaded area in plots (*a*)–(*e*) designates where the effect of the peak has a significant effect on the synthetic data, so direct comparisons between the observations and the models cannot be made here.

tangency radius of this spectrometer chord (1.205 m) and the sawtooth inversion radius (1.16 m). When we compare the drops in FIDA emission with the three sawtooth models, it is evident from figure 9(*d*) that all of them predict a drop in emission that is smaller than the measured value. In making these comparisons, it should be noted that while finite Larmor radius corrections are taken into account in NUBEAM for the purpose of evaluating neutralisation probabilities and collision rates, they are not taken into account in terms of the local magnetic field used to track particle orbits, since a guiding centre approximation is used [16]. This introduces an error in the synthetic spectra for tangency radii lying close to the boundary of the sawtoothing region. The discrepancy between measurements and modelling in figure 9(*d*) could perhaps be due to a pitch angle (*i.e.* Larmor radius) dependence of the effects of the sawtooth on the fast ion population that is not captured by any of the models, although further investigation would be needed to confirm this. Figure 9(*d*) shows the largest drop in the observed FIDA radiance across all valid channels, along with the largest drop in the ergodic and Porcelli models. Figure 9(*e*) shows the largest drop in the Kadomtsev model, with similar drops in the other models to figure 9(*d*). This is somewhat counter-intuitive: it may be thought that channels corresponding to locations closer to the core would have larger drops in radiance, since the core is inside the sawtoothing region and contains more fast ions prior to the crash. The drop in radiance in the channel used in figure 9(*e*) and the lesser drops in other channels can be correlated with the change in the fast-ion distributions predicted by TRANSP/NUBEAM due to the good correspondence between the observed and predicted values. Figure 10 shows the computed fast-ion distributions at a major radius of 1.205 m in the midplane of the tokamak (the Kadomtsev model is used here, as an example). Pitch here is defined as the ratio of the component of the marker's velocity parallel to the magnetic field to the full velocity. On MAST during conventional operation the toroidal component of the magnetic field, B_ϕ, was directed clockwise as seen from above and current anti-clockwise, so particles with negative pitch are travelling in the co-current direction. The overlaid contours show the extent of the *weight function* for the FIDA diagnostic [14, 22], specifically in the chosen spatial location and over the range of wavelengths that are dominated by the presence of the fast ions. Weight functions are essentially a measure of the probability that a CX reaction emits a photon of a specific wavelength (or range of wavelengths), given the velocity of the fast ion and the angle of the diagnostic line-of-sight to the local magnetic field [23, 24].

For comparison with figure 9(*e*) the relative change in the fast-ion distributions across the three models is shown in figure 11.

It can be observed across all of the models in figure 11 that there is a significant loss of fast ions (up to 50 %) from energies between 45–55 keV across pitches between -0.25 and -1, with the Kadomtsev (figure 11(*a*)) model showing additional losses down to 30 keV and the ergodic (figure 11(*b*)) and Porcelli (figure 11(*c*)) models showing an increase in the fast ions around a pitch of -0.75 across energies 25–40 keV. Additionally there is an increase in fast ions with energies less than 20 keV across positive pitch values. The higher energy particles are expelled from the sawtoothing region during the crash and lower energy particles from larger radii are mixed in. These lower energy fast ions will have undergone significant pitch angle scattering. The apparent preference for positive pitch angle after the crash across the models in figure 11 is likely to be an artefact of the normalisation. It can be seen that the weight function primarily intersects the region of significant loss, which is reflected in the decrease in FIDA radiance shown in figure 9, with the smaller regions of increase within the intersection

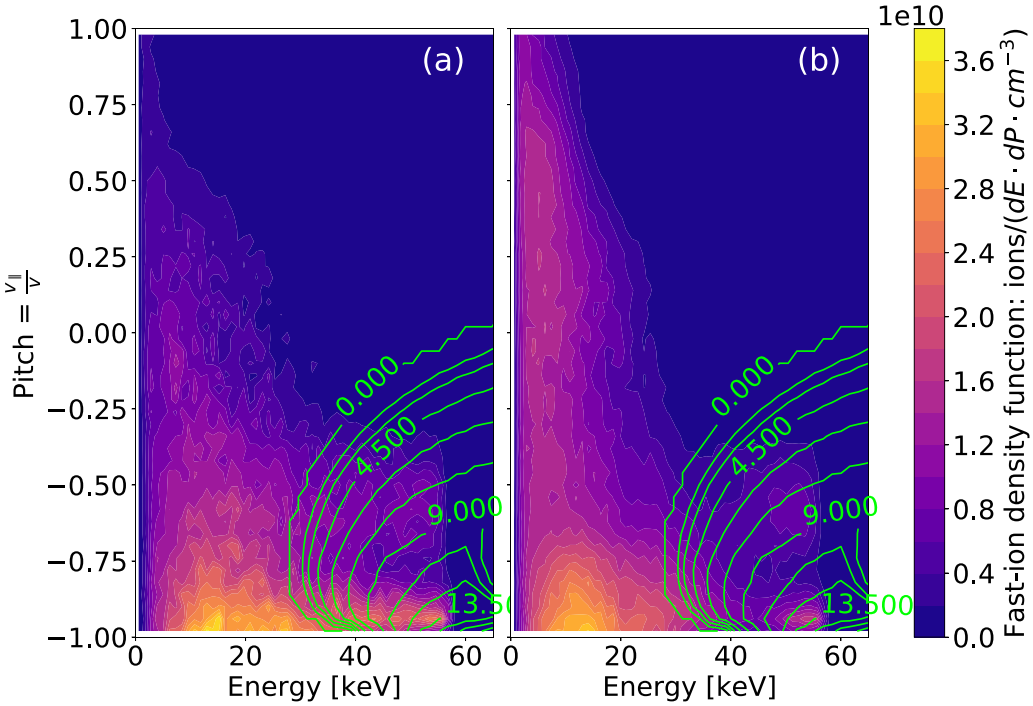

Figure 10. Simulated fast ion distributions for $R = 1.205$ m in the device midplane using the Kadomtsev model. (*a*) Before crash, (*b*) after crash. The green contours represent the weight function for the FIDA diagnostic in the fast-ion dominated wavelength range and the spatial location of measurement.

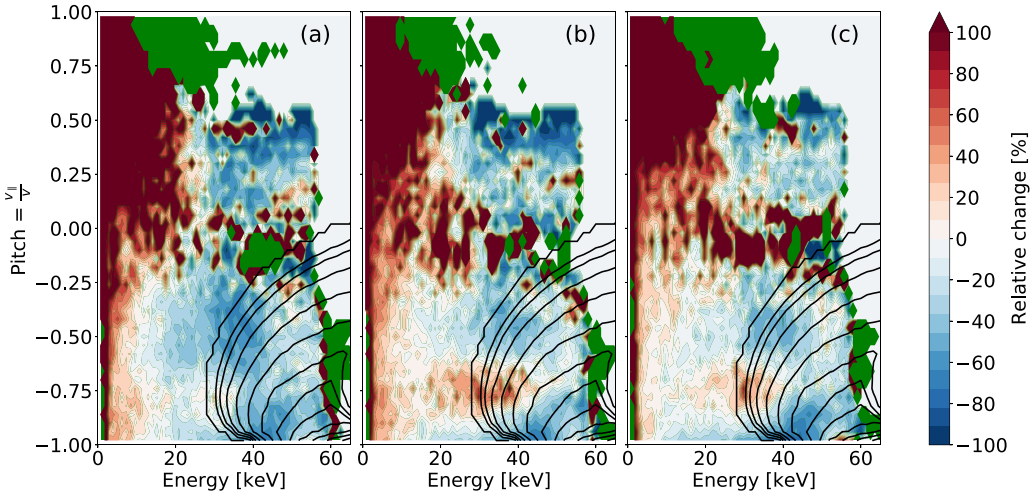

Figure 11. The relative change in the fast-ion distribution function for $R = 1.205$ m in the device midplane. (*a*) Kadomtsev, (*b*) ergodic, (*c*) Porcelli. Areas in green represent phase-space regions with a fast-ion presence after the crash that had no presence before. Note that in some regions there is a positive change of greater than 100 %. The black contours represent the weight function for the FIDA diagnostic in the fast-ion dominated wavelength range and the spatial location of measurement.

present in the ergodic and Porcelli models leading to the smaller decrease present in those models compared to the Kadomtsev. The shape of the weight function depends on the angle between the line-of-sight and the magnetic field, and hence is channel-dependent. In the other channels the weight function primarily intersects the population of newly injected fast ions around 55 keV, so in these channels a smaller change in FIDA radiance due to redistribution of the FI population by the sawtooth is observed. It should be emphasised when examining synthetic fast-ion distributions that any regions of the phase-space outside of the overlap with the weight function cannot be probed with the FIDA diagnostic, so cannot be compared with experimental values. The recovery of the fast-ion distribution after the crash can be observed in figure 12, where the spectra move towards pre-crash conditions as the time window averaged for the 'after' portion of the data moves further from the crash. The total time interval covered in this figure is comparable to the fast-ion slowing down time, which is the timescale on which we could expect the fast-ion distribution to recover following a sawtooth crash. Figure 4(*b*) shows an

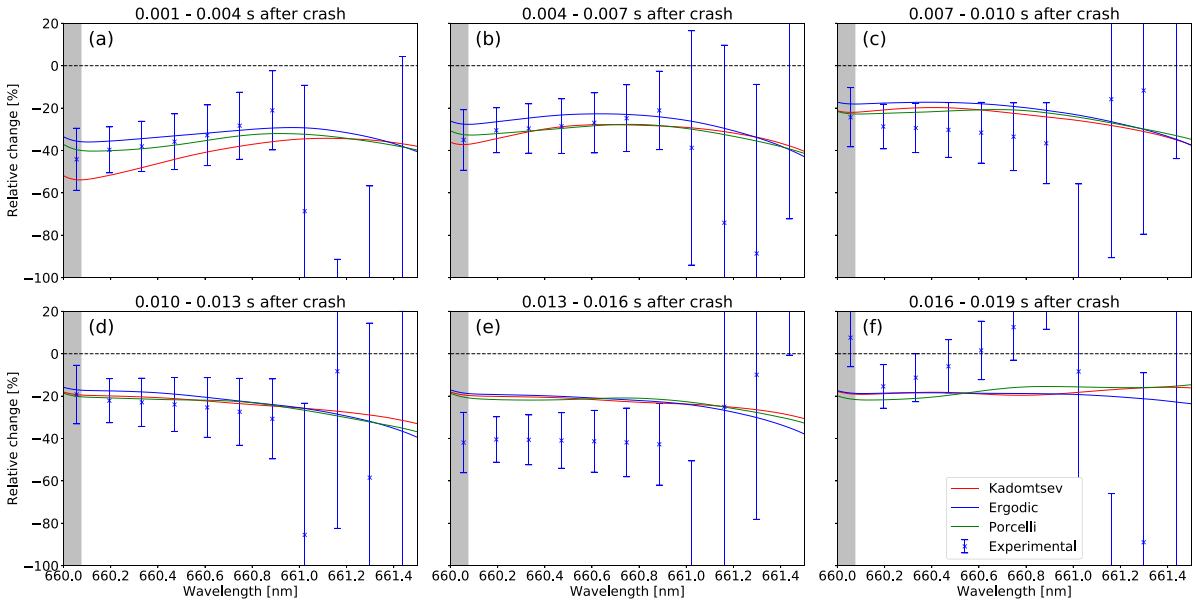

Figure 12. Relative change in the spectral radiance at $R = 1.205$ m in the device midplane, averaged over the indicated time windows. Note that figure 12(*a*) examines the same data as figure 9(*e*).

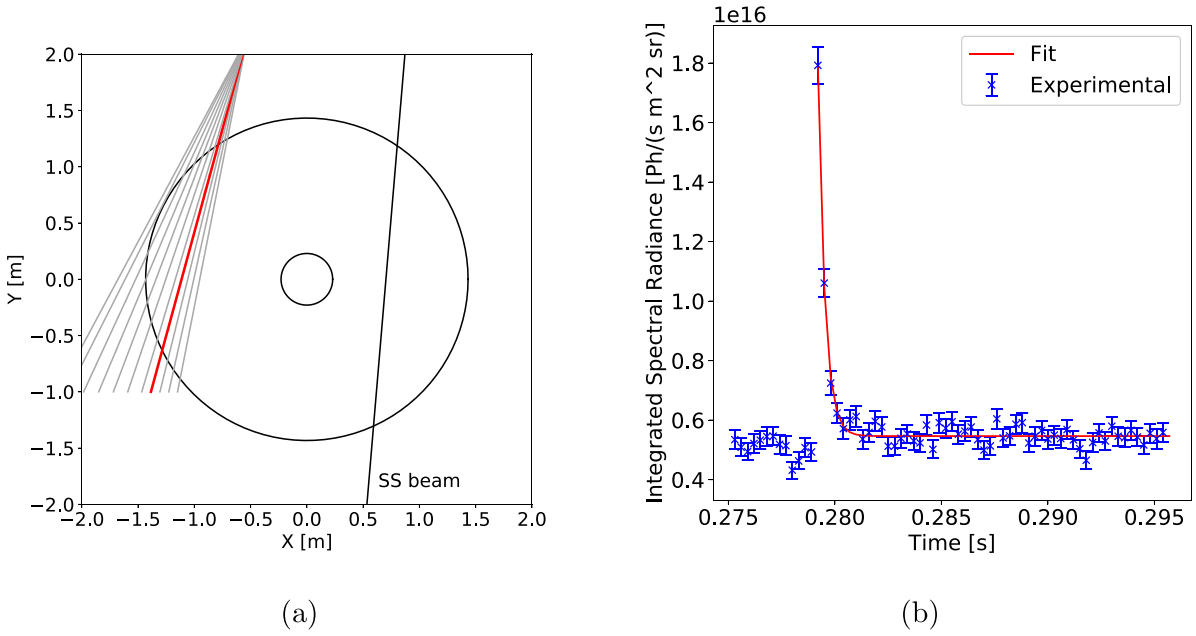

Figure 13. (*a*) Available toroidally-viewing passive chords, with selected chord highlighted in red, and the NBI beamline to emphasise the passive nature of the view. Data from this chord is shown in figure 13(*b*). The black circles show the minimum and maximum extent of the plasma. (*b*) Spike and decay of passive signal seen during a sawtooth crash. The decaying part of the signal has been fitted with an exponential.

overall degradation of the fast-ion confinement, which could contribute to the incomplete recovery of the spectra. There is a significant disagreement between the experimental and synthetic data in figure 12(*e*). While we do not yet have a definitive explanation for this, examination of the D-α signal for one of the three pulses (#29 880) in the period after the third sawtooth shows a significant increase around the start of this averaging window. This could be a consequence of more edge neutrals permeating into the hot plasma, which would be likely to generate an increase in the passive FIDA signal, thereby affecting the passive subtraction. Such an effect was not taken into account in the FIDASIM calculation for these pulses.

5. Passive FIDA

As described in section 2 there is a FIDA spectral component generated by charge exchange reactions between fast ions and neutrals present in the colder edge region of the plasma,

rather than the beam neutrals. In this section, the effect of the sawtooth crashes (in #29 880) on the passive emission observed by a toroidally directed passive view on MAST is examined. Figure 13 shows a plan view of the MAST plasma, with the black circles denoting the minimum and maximum extent of the plasma at the chosen time. The fan of chords available to the passive FIDA view are shown in grey, with an example channel shown in red. Figure 13 shows the integrated radiance, I, for this channel for a single sawtooth crash. A decaying exponential of the form:

$$I(t) = ae^{-\frac{(t-t_0)}{\tau}} + c \quad (1)$$

where t is time, t_0 is a time offset, and a, c and τ are constants, is used to describe the radiance temporal decay. We fit the decay time τ to the decaying part of the signal. It is observed that there is a large spike in integrated radiance across all channels that intersect the plasma, with decay times between 0.3–0.5 ms. This feature is not observed in data integrated in regions free from FIDA light, indicating that background fluctuations are not the cause. Therefore the data suggests that there is a sudden significant increase in the population of passing fast ions followed by a rapid decrease. It is likely that this rapid decrease is due primarily to charge exchange between these passing fast ions and edge neutrals rather than direct fast ion orbit losses. A typical neutral density, n_0, in the MAST plasma edge is a few times $1 \times 10^{16}\,\mathrm{m}^{-3}$ [25]: using the velocity, v, and charge exchange cross-section σ for a 40 keV deuteron [26], we estimate the charge-exchange time to be $\tau_{CX} = 1/(vn_0\sigma) \sim 0.3$ ms, consistent with the decay time in figure 13. Bolte *et al* [27] have carried out a detailed examination of passive FIDA emission on the DIII-D tokamak, where they also observe the preference for the ejection of passing particles from the core to the edge. Additionally, they are able to determine, with an accurately calibrated diagnostic and the use of passive FIDASIM simulations, that approximately 1 % of the fast-ion population is expelled into the edge region. Looking to the future, MAST-Upgrade will have a fast-ion loss detector, which is expected to provide direct information on sawtooth-induced fast-ion losses.

6. Conclusion

Based on forward modelling performed with the FIDASIM code in conjunction with experimental FIDA data it is not possible to distinguish between complete (Kadomtsev and ergodically mixed Kadomtsev) and incomplete (Porcelli) reconnection models for the sawtooth crashes, due to the level of noise present in the FIDA data and the relatively small differences seen in the FIDASIM data between the models. While issues regarding the calibration of the diagnostic mean that there are significant difficulties in analysing the absolute FIDA radiances, examining the relative change in the spectra and synthetic fast-ion distribution resulting from the sawtooth crashes allows for further investigation into the fast-ion redistribution. Large drops in the measured spectral radiance are reflected in the synthetic spectra, which indicates significant depletion of the fast-ion phase-space at energies around 40 keV, which progressively recovers over the inter-sawtooth period. Passive data show that sawtooth crashes lead to a sudden increase and subsequent rapid decay of passing fast ions in the edge region of the plasma. We conclude that additional fast ion diagnostics, such as those that will be available in MAST-Upgrade, are likely to be required in order to discriminate experimentally between alternative models of fast ion redistribution and loss resulting from sawtooth crashes.

Acknowledgments

This work has been carried out within the framework of the EUROfusion Consortium and has received funding from the Euratom research and training programme 2014-2018 and 2019-2020 under Grant Agreement No. 633053. The views and opinions expressed herein do not necessarily reflect those of the European Commission. Funding from EPSRC grant number EP/T012250/1 is acknowledged. CM was supported by US DOE grant number DE-SC0019007.

ORCID iDs

A.R. Jackson https://orcid.org/0000-0002-3814-5083
A.S. Jacobsen https://orcid.org/0000-0002-9033-1094
K.G. McClements https://orcid.org/0000-0002-5162-509X
C.A. Michael https://orcid.org/0000-0003-1804-870X
M. Cecconello https://orcid.org/0000-0002-2571-1920

References

[1] von Goeler S., Stodiek W. and Sauthoff N. 1974 Studies of Internal Disruptions and m=1 Oscillations in Tokamak Discharges with Soft—X-Ray Techniques *Phys. Rev. Lett.* **33** 1201–3
[2] Wising F., Anderson D. and Lisak M. 1992 Modelling of fast ion redistribution due to sawteeth in neutral beam heated plasmas *Plasma Phys. Control. Fusion* **34** 853–62
[3] Chapman I.T. *et al* 2007 The physics of sawtooth stabilization *Plasma Phys. Control. Fusion* **49** B385–B394
[4] Chapman I.T. *et al* 2010 Empirical scaling of sawtooth period for onset of neoclassical tearing modes *Nucl. Fusion* **50** 102001
[5] Pace D.C. *et al* 2011 Transport of energetic ions due to sawteeth, Alfvén eigenmodes and microturbulence *Nucl. Fusion* **51** 043012
[6] Muscatello C.M., Heidbrink W.W., Kolesnichenko Y.I., Lutsenko V.V., Van Zeeland M.A. and Yakovenko Y.V. 2012 Velocity-space studies of fast-ion transport at a sawtooth crash in neutral-beam heated plasmas *Plasma Phys. Control. Fusion* **54** 025006
[7] Weiland M., Geiger B., Jacobsen A.S., Reich M., Salewski M. and Odstrčil T. 2016 Enhancement of the FIDA diagnostic at ASDEX Upgrade for velocity space tomography *Plasma Phys. Control. Fusion* **58** 025012
[8] Salewski M. *et al* 2016 High-definition velocity-space tomography of fast-ion dynamics *Nucl. Fusion* **56** 106024
[9] Liu D., Heidbrink W.W., Podestà M., Hao G.Z., Darrow D.S., Fredrickson E.D. and Kim D. 2018 Effect of sawtooth

crashes on fast ion distribution in NSTX-U *Nucl. Fusion* **58** 082028
[10] Madsen B., Salewski M., Huang J., Jacobsen A.S., Jones O. and McClements K.G. 2018 Velocity-space tomography using prior information at MAST *Rev. Sci. Instrum.* **89** 1–6
[11] Cecconello M. *et al* 2015 Energetic ion behaviour in MAST *Plasma Phys. Control. Fusion* **57** 014006
[12] Cecconello M., Sperduti A. and the MAST team 2018 Study of the effect of sawteeth on fast ions and neutron emission in MAST using a neutron camera *Plasma Phys. Control. Fusion* **60** 055008
[13] Heidbrink W.W. 2010 Fast-ion Dα measurements of the fast-ion distribution *Rev. Sci. Instrum.* **81** 10D727
[14] Michael C.A. *et al* 2013 Dual view FIDA measurements on MAST *Plasma Phys. Control. Fusion* **55** 095007
[15] Hawryluk R.J. 1981 An empirical approach to tokamak transport *Phys. Plasmas Close Thermonucl. Conditions* **1** 19–46
[16] Pankin A., McCune D., Andre R., Bateman G. and Kritz A. 2004 The tokamak Monte Carlo fast ion module NUBEAM in the national transport code collaboration library *Comput. Phys. Commun.* **159** 157–84
[17] Heidbrink W.W., Liu D., Luo Y., Ruskov E. and Geiger B. 2011 A code that simulates fast-ion Dα and neutral particle measurements *Communications Computational Phys.* **10** 716–41
[18] Kadomtsev B.B. 1975 On the tearing instability in tokamaks *Fiz. Plazmy* **1** 710–14
[19] Porcelli F., Boucher D. and Rosenbluth M. 1996 Model for the sawtooth period and amplitude *Plasma Phys. Control. Fusion* **38** 2163–86
[20] Podesta M. 2019 Private communication
[21] McCune D. 2005 NTCC module – kdsaw – Kadomtsev Sawtooth Model with Porcelli Upgrade (https://w3.pppl.gov/ntcc/KDSAW/DOC)
[22] Heidbrink W.W., Luo Y., Burrell K.H., Harvey R.W., Pinsker R.I. and Ruskov E. 2007 Measurements of fast-ion acceleration at cyclotron harmonics using Balmer-alpha spectroscopy *Plasma Phys. Control. Fusion* **49** 1457–75
[23] Salewski M. *et al* 2014 On velocity-space sensitivity of fast-ion D-alpha spectroscopy *Plasma Phys. Control. Fusion* **56** 105005
[24] Jacobsen A.S. 2015 Methods to determine fast-ion distribution functions from multi-diagnostic measurements *PhD dissertation*, Technical University of Denmark
[25] McClements K.G., Tani K., Akers R.J., Liu Y.Q., Shinohara K., Tsutsui H. and Tsuji-Iio S. 2018 The effects of resonant magnetic perturbations and charge-exchange reactions on fast ion confinement and neutron emission in the Mega Amp Spherical Tokamak *Plasma Phys. Control. Fusion* **60** 095005
[26] Wesson J. 2004 *Tokamaks* 3rd ed (Oxford: Oxford University Press)
[27] Bolte N.G., Heidbrink W.W., Pace D., Van Zeeland M. and Chen X. 2016 Measurement and simulation of passive fast-ion D-alpha emission from the DIII-D tokamak *Nucl. Fusion* **56** 112023